www.lajss.org
Latin American Journal of Solids and Structures 5 (2008)259–287

Energy absorption characteristics of aluminum plates subjected to projectile impact

M. A. Iqbal[a,*] and N. K. Gupta[b]

[a]Department of Civil Engineering, I. I. T. Roorkee, Roorkee-247667, India.
Email: iqbal_ashraf@rediffmail.com
[b]Department of Applied Mechanics, I. I. T. Delhi, Hauz Khas New Delhi-110016, India.
Tel.: +91-1332-285866; Fax: +91-1332-275568

Abstract

This paper presents a detailed investigation of energy absorption characteristics of thin single as well as layered in-contact aluminum target plates of different thicknesses impacted by blunt, ogive and hemispherical nosed steel projectiles. Influence of various parameters affecting the energy absorption capacity of the target, such as kinetic energy of the impacting projectile and its nose shape, configuration of the target plate, its mode of failure as well as thickness of the target plate was studied. The extent of energy absorption of the target plate was found to be highly influenced by its failure mechanism. It offered higher perforation resistance when the failure occurred through "bending" and "tensile stretching" than when it failed through "shear plugging". Effect of target configuration was studied by varying the number of layers and individual plate thickness keeping a given constant overall target thickness. The absorbed energy was found to decrease with an increase in the number of layers, which revealed that the monolithic target plate offered highest resistance against projectile perforation. The experimental findings were also verified with the numerical simulations carried out using finite element code ABAQUS. Energy absorption capacity of the target plates obtained from the numerical analysis was found in good agreement with the experimental observations.

Keywords: Kinetic energy, Projectile perforation, Ballistic limit, layered plate.

1 Introduction

The study of energy absorption behavior of metallic plates subjected to projectile impact requires attention due to the wide range of applications and complex nature of the problem. Extensive research has been carried out in the past [9, 11] to understand various features of this complex phenomenon both from the point of view of the projectile as well as the target plate by using different impact conditions and varying target configuration.

*Corresp. author. Email: iqbalfce@iitr.ernet.in. Received 6 July 2008; In revised form 6 Oct 2008

Marom and Bonder [9] carried out analytical and experimental studies on the ballistic resistance of thin, flat beams of pure aluminum and 6061-T6 aluminum alloy, arranged in various in-contact as well as spaced layers, and impacted by 0.22 in caliber projectiles. The multi-layered in-contact beams showed greater resistance to penetration than the equivalent monolithic beams. Dey et al. [14] studied the ballistic response of Weldox 700 E steel plates impacted in single and layered configuration by blunt and ogive nosed projectiles. For blunt nosed projectile impact two layered plate of 6 mm thickness showed better resistance than 12 mm thick monolithic plate. However, when the two layers of 6 mm thickness were separated by 24 mm air gap the ballistic resistance was found to be greater than that of the monolithic plate of 12 mm thickness but lesser than that of the two layered in-contact plate of 6 mm thickness. For ogive nosed projectiles however, the monolithic plates showed highest ballistic resistance followed by layered in-contact plates and layered spaced plates respectively.

Zaid et al. [2] compared the deformation profiles and strain induced in 2.5 mm mild steel plates when impacted by blunt projectiles of 10 mm diameter with the results of static tests and found that bulging of the target plates reduces drastically at velocities above the ballistic limit. It was concluded that energy absorbed by the target plates during perforation is less than the energy absorbed when the projectile is embedded in the plate. Gupta et al. [12] observed that defuse and global deformation of 1100-H12 aluminum target plates decreases with an increase of projectile impact velocity and increases with an increase of target thickness. Wen and Jones [8] used dimensional analysis and proposed a semi-empirical equation for the perforation energy during impact of mild steel plates struck by blunt projectiles. Energy absorbed by global structural response, including bending and stretching, and energy absorbed in shearing out a plug of diameter equal to that of the projectile were taken care of in the formulation. The results from solution of this equation compared well with the test results at low impact velocities. Dey et al. [13] studied the effect of target strength of 12 mm thick steel plate of varying hardness impacted by blunt, conical and ogive nosed projectiles. Despite the large difference of yield strength of targets there was not much difference between the ballistic limit of the same projectile nose shape.

Corran et al. [4] investigated the effect of projectile nose shape on penetration of steel and aluminum alloy plates using blunt and cylindro-conical projectiles of 12.5 mm diameter. Mass of the projectiles was varied from 15 to 100 grams and impact velocity from 50 to 250 m/s. It was observed that critical impact energy is dependent on projectile nose radius, being maximum corresponding to a nose radius at which the mode of failure changes from shear plugging to tensile stretching. Othe et al. [15] estimated the critical fracture energy of 7 to 38 mm thick carbon steel plates impacted normally by heavy, blunt, hemispherical, and conical nosed steel projectiles of diameter varying from 66 to 160 mm. Impact velocity of the projectiles varied from 25 to 170 m/s. It was found that conical projectiles are efficient penetrators. As their nose angle is decreased, the perforation resistance of the target tends to drop. The critical perforation energies were found to be equal for blunt and hemispherical projectiles. Gupta et al. [11] investigated the behavior of 1 mm thick aluminum target plates impacted by blunt

and hemispherical nosed projectiles. Blunt nosed projectile was more effective to perforate the target plates. Numerical analysis was carried out using a commercial finite element code ABA QUS/Explicit, the results obtained from the numerical simulation were found in good agreement with those of the experimental results. Size of element was found to be an important parameter affecting the numerical results. Adaptive meshing was used to obtain economic solution and to avoid premature termination of the problem. Gupta et al. [12] studied the effect of projectile nose shape impact velocity and target thickness on the deformation behavior of aluminum target plates through experimental and numerical investigations. Hemispherical nosed projectile was found to be the least efficient perforator while it caused highest plastic deformation of the target plates. The ballistic limit of 0.5, 0.71, 1.0 and 1.5 mm thicknesses was found to be higher for blunt nosed projectile impact, however, the ballistic limit of 2.0, 2.5 and 3.0 mm thicknesses was higher for ogive nosed projectile impact. The predicted residual velocities as well as the ballistic limit velocity of the projectiles were also found to compare well with those of the experimental observations. Dey et al. [13] observed that ballistic limit velocity of the blunt projectiles decreases with increasing yield strength of steel target plates, while for ogive and conical projectiles an opposite trend was observed. Numerical investigations of some experiments showed that the experimental observation of increase in the ballistic limit velocity with increasing target strength for conical projectiles was well predicted by the code but the decrease of ballistic limit velocity for blunt nosed projectile could not be predicted. Dey et al. [14] studied the ballistic response of Weldox 700 E steel plates. The ballistic limit of 6 mm and 12 mm thick monolithic target plates was found to be higher for ogive nosed projectile impact than that of the blunt nosed projectile impact.

The results obtained from the previous studies [9, 11] provide significant information pertaining to the factors affecting the energy absorption behavior of metallic plates, such as, failure mode, thickness of target plate and its configuration, kinetic energy and nose shape of the impacting projectile, and, global and localised plastic deformation of the target plate. However, the influence of each of the abovementioned parameters on the energy absorption capacity of the target plate is quite significant, and hence, this subject requires further investigation. The present study is based on the kinetic energy absorption characteristics of single and layered in-contact aluminum alloy (1100-H12) target plates of 0.5, 0.71, 1.0, 1.5, 2.0, 2.5 and 3 mm thicknesses impacted by blunt, ogive and hemispherical nosed hardened steel projectiles of 19 mm diameter. These projectiles were normally impacted with different kinetic energies on the target plates, arranged in single and layered combinations, and the energy absorbed by the target plate as well as the residual energy of the projectile, if perforated, was obtained.

Energy absorbed by the target plate was found to increase initially with an increase in the impact energy of the projectile, however, with further increase in the projectile impact energy the energy absorbed by the target plate decreased. Nose shape of the projectile was found to have a significant effect on the energy absorption capacity of the target plate as the failure mode of the target plate was highly sensitive to projectile nose shape. Single plate was found to offer more resistance against the perforation of the projectile as compared to layered plate of

same total thickness. Numerical simulation of the problem was also carried out to compare the computational results with those of the experimental observations. The flow stress as well as fracture strain model proposed by [6,7] was incorporated to simulate the behavior of the target material. The detail of material parameters obtained for the effective implementation of the Johnson-Cook model is presented in [11]. Finite element package ABAQUS/Explicit (version 6.3) was used to simulate the experiments. The energy absorption capacity of the target plates obtained through numerical simulations was found in good agreement with the experimental results.

2 Experimental and Numerical Investigations

A detailed experimental investigation was carried out to describe the kinetic energy absorption behavior of the single and layered aluminum target plates. Circular target plates of 255 mm span diameter procured in seven different thicknesses namely 0.5, 0.71, 1.0, 1.5, 2.0, 2.5 and 3 mm were normally impacted by blunt, ogive and hemispherical nosed projectiles of 19 mm diameter and 52.5 grams mass. The projectiles were made hollow with a slight variation in their wall thickness in order to obtain the constant mass. A pressure gun capable to launch the projectile of aforesaid mass in the sub-ordnance velocity range (33-126 m/s) was used for this purpose. Impact and residual velocity of the projectile was obtained and energy absorbed by the target plate was evaluated (Absorbed Energy = Impact Energy - Residual Energy). The observed and predicted impact energy of the projectile, and the energy absorbed by the target plate is shown in Table 1 for different thicknesses of the single and layered target plates of varying configuration. It was observed that each of the three projectiles deformed the target plate in a distinct fashion as is depicted from the deformed specimens shown in Fig. 1.

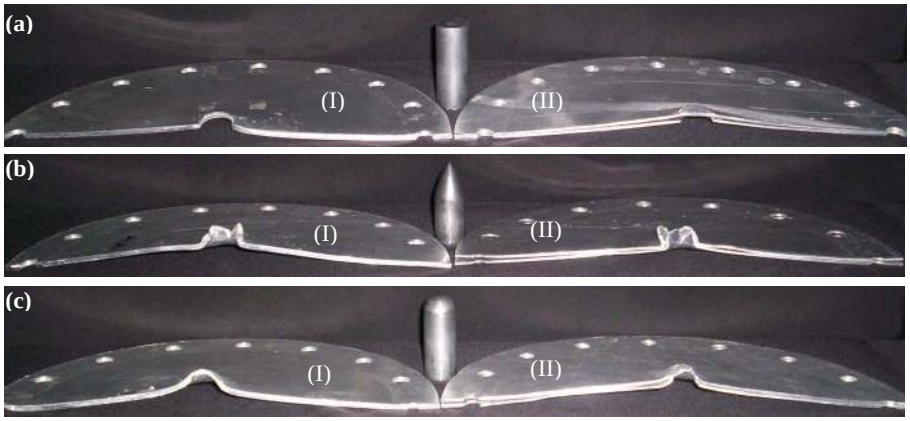

Figure 1: Deformed targets (I) Single plate of 3 mm thickness (II) Two layers of 1.5 mm thickness, impacted by projectiles with nose shape: (a) Blunt, (b) Ogive and (c) Hemispherical

Table 1: Observed and predicted Impact Energies (IE) of Blunt, Ogive and Hemispherical nosed Projectiles as well as Energy Absorbed (AE) by the target plates.

Target Thickness (mm)	No. of layers	Blunt nosed Projectile				Ogive nosed projectile				Hemispherical nosed projectile			
		Observed		Predicted		Observed		Predicted		Observed		Predicted	
		IE	AE	IE	AE	IE	AE	IE	AE	IE	AE	IE	AE
		(Joule)				(Joule)				(Joule)			
0.5	1	337.74	60.28	337.74	40.84	305.08	45.59	305.08	40.03	369.38	66.28	369.38	60.99
		316.41	70.9	316.41	50.75	251.51	44.89	251.51	50.67	331.81	73.15	331.81	70.29
		285.54	74.21	285.54	64.16	224.41	48.83	224.41	58.54	265.46	73.46	265.46	76.81
		269.1	75.95	269.1	77.15	184.74	61.79	184.74	71.86	232.81	83.95	232.81	88.01
		217.38	70.19	217.38	80.61	157.3	68.33	157.3	78.92	201.05	79.91	201.05	84.21
		207.16	72.57	207.16	83.94	127.3	66.53	127.3	73.34	178.36	78.2	178.36	87.28
		169.88	77.63	169.88	85.29	102.45	62.91	102.45	68.17	161.89	78.74	161.89	89.89
		142.48	77.52	142.48	84.19	76.83	56.79	76.83	61.76	129.55	76.54	129.55	87.96
		113.64	74.56	113.64	82.53	59.14	51.42	59.14	53.97	111.69	76.72	111.69	85.12
		94.14	74.83	94.14	78.26	43.4	41.71	43.26	43.26	86.57	69.73	86.57	73.91
		60.3	57.19	60.3	58.36	29.89	29.89			61.81	57.48	61.81	59.48
		33.21	33.21	48.98	48.98					47.08	47.08	53.39	53.39
	2	382.04	91.07	382.04	70.12	354.43	65.23	354.43	39.79	376.87	107.07	376.87	101.12
		354.04	93.99	354.04	75.58	320.21	73.66	320.21	58.29	331.55	120.22	331.55	123.29
		340.67	101.21	340.67	87.28	281.31	87.71	281.31	74.19	300.99	123.14	300.99	128.53
		304.68	108.57	304.68	96	238.22	94.5	238.22	87	296.11	124.37	296.11	132.78
		252.88	104.42	252.88	105.38	210.5	101.31	210.5	92.62	251.04	129.57	251.04	141.76
		223.81	106.22	223.81	110.6	192.39	107.42	192.39	102.6	214.28	126.42	214.28	138.91
		205.46	109.54	205.46	114.68	157.26	108.11	157.26	101.4	181.99	130.83	181.99	133.35
		173.62	109	173.62	121.4	109.07	92.2	109.07	85.88	153.88	130.35	153.88	135.16
		117.59	94.54	117.59	99.85	78.74	74.96	78.74	72.96	111.83	106.81	111.83	110.19
		68.86	68.86	90.24	90.24	40.31	40.31	44.77	44.77	75.6	75.6	102.21	102.21
	3	366.76	110.68	366.76	96.809	374.35	97.76	374.35	62.67	387.01	149.95	387.01	157.74
		333.41	116.36	333.41	103.73	339.39	100.02	339.39	74.31	345.67	159.36	345.67	168.26
		285.94	114.58	285.94	106.85	320.91	102.59	320.91	88.63	315.69	164.89	315.69	177.7
		220.12	111.14	220.12	118.01	290.07	113.52	290.07	105.9	265.71	162.29	265.71	173.1
		213.33	131.38	213.33	121.28	250.03	119.3	250.03	126.2	250.17	159.65	250.17	171.35
		188.32	130.51	188.32	120.14	227.83	124.8	227.83	131.1	229.99	154.87	229.99	168.4
		164.62	122.37	164.62	117.37	194.75	129.15	194.75	139.8	190.76	153.08	190.76	161.2
		119.85	107.99	119.85	101.82	137.02	112.41	137.02	118	161.93	146.09	161.93	150.14
		83.44	83.44	93.24	93.24	116.9	107.85	116.97	111.6	111.52	111.52	129.36	129.36
						68.17	68.17	91.99	91.99				
	4	371.91	151.65	371.91	138.05	393.76	142.1	393.76	101.36	344.44	162.22	344.44	180.47
		324.97	147.47	324.97	142.46	347.38	156.19	347.38	133.39	327.32	171.9	327.32	183.68
		314.88	149.43	314.88	144.25	299.27	154.54	299.27	132.38	299.53	175.37	299.53	186.59
		276.65	148.59	276.65	155.57	288.8	155.41	288.8	137.44	253.32	173.89	253.32	183.62
		249.27	148.77	249.27	156.86	253.55	157.66	253.55	141.09	240.73	172.69	240.73	181.31
		224.95	149.37	224.95	154.46	201.84	142.28	201.84	129.29	219.58	168.39	219.58	180.02
		193.64	148.6	193.64	154.21	165.76	131.5	165.76	125.98	188.62	163.99	188.62	171.65
		143.03	128.42	143.03	132.41	119.64	110.44	119.64	107.94	148.56	148.56	161.35	161.35
		105.06	105.06	118.54	118.54	99.9	99.9	96.71	96.71				
	5	367.06	154.49	367.06	160.16	363.41	159.09	363.41	140.63	394.64	192.2	394.64	213.02
		337.31	163.76	337.31	174.76	340.43	163.01	340.43	153.4	354.91	190.18	354.91	210.78
		300.37	162.22	300.37	176.06	292.34	165.22	292.34	164.21	308.14	195.42	308.14	211.48
		290.31	163.91	290.31	175.26	254.35	158.47	254.35	158.9	292.97	206.41	292.97	217.99
		275.99	168.41	275.99	182.1	236.31	159.46	236.31	162.66	249.89	200.35	249.89	209.6
		240.31	166.67	240.31	176.84	184.01	149.01	184.01	157.9	223.79	190.29	223.79	197.05
		182.74	158.37	182.74	165.94	152.68	136.69	152.68	141.33	195.13	179.35	195.13	184.67
		129.49	129.49	162.25	162.25	114.31	114.31	126.65	126.65	165.36	165.36	178.66	178.66
0.71	1	342.95	114.71	342.95	93.75	346.78	64.37	346.79	73.8	349.04	72.35	349.03	91.99
		267.83	106.76	267.83	94.98	323.78	64.5	323.78	75.64	329.32	80.32	329.32	103.29
		253.5	112.14	253.5	98.74	278.52	63.89	278.52	84.34	254.9	79.13	254.9	100.53
		249.54	116.22	249.54	101.93	251.51	69	251.51	98.97	214.44	82.57	214.44	99.29
		177.41	92.86	177.41	85.61	204.78	76.22	204.78	101.6	165.54	95.78	165.54	104.65
		152.48	102.11	152.48	90.11	137.06	75.11	137.06	89.01	134.67	87.96	134.67	96.75
		109.29	88.26	109.29	83.68	110.88	71.24	110.88	84.42	112.14	87.25	112.14	91.43
		69.45	65.47	69.45	65	68.94	58.87	68.94	63.81	78.29	72.66	78.29	74.38
		48.07	48.07	51.51	51.51	51.41	49.52	51.41	51.41	62.72	62.72	69.35	69.35
						38.71	38.71						

Continued on next page

Table 1 – continued from previous page

Target Thickness (mm)	No. of layers	Blunt nosed Projectile				Ogive nosed projectile				Hemispherical nosed projectile			
		Observed		Predicted		Observed		Predicted		Observed		Predicted	
		IE	AE	IE	AE	IE	AE	IE	AE	IE	AE	IE	AE
		(Joule)				(Joule)				(Joule)			
	2	361.35	130.55	361.35	114.35	329.03	92.12	329.03	74.79	349.05	146	349.05	156.26
		331.49	133.15	331.49	123.05	290.12	99.35	290.12	87.91	304.05	160.97	304.05	172.92
		318.36	136.21	318.36	132.28	264.45	98.12	264.45	96.75	276.51	158.69	276.51	172.1
		280.08	134.06	280.08	136.42	235.06	103.6	235.06	99.84	247.82	161.22	247.82	170.22
		233.13	131.49	233.13	143.07	225.4	112.67	225.4	103.85	227.27	157.64	227.27	166.96
		220.48	137.63	220.48	143.27	201.21	118.66	201.21	115.03	202.22	149.77	202.22	159.07
		194.76	140.26	194.76	142.81	164.94	115.19	164.94	109.41	170.83	141.6	170.83	149.52
		162.23	134.94	162.23	136.7	141.71	109.85	141.71	107.99	138	126.72	138	131.37
		126.31	114.69	126.31	119.08	110.09	98.36	110.09	97.2	105.23	105.23	122.45	122.45
		105.55	101.23	99.93	99.93	85.502	83.01	85.5	83.71				
		83.88	83.88			68.7	68.7	78.25	78.25				
	3	378.36	156.97	378.36	132.26	344.63	126.73	344.63	107.5	379.99	153.48	379.99	173.26
		339.69	158.24	339.69	143.09	310.33	139	310.33	124.63	345.68	181.96	345.68	190.44
		305.46	155.56	305.46	145.31	282.18	146.06	282.18	141.36	313.15	183.76	313.15	198.92
		260.75	154.25	260.75	146.57	242.28	142.9	242.28	146.01	260.78	177.86	260.78	189.81
		228.46	147.11	228.46	143.27	235.28	156.12	235.28	158.79	231.35	171.7	231.35	183.64
		211.17	150.62	211.17	144.9	199.74	146.31	199.74	153.71	191.75	158.99	191.75	167.69
		179.4	138.58	179.4	140.59	174.43	141.92	174.43	147.06	162.32	146.81	162.32	152.43
		153.37	131.56	153.37	133.91	149.38	132.69	149.38	137.01	153.49	143.81	153.49	148.35
		125.63	117.1	125.63	119.72	125.61	119.84	125.61	122.43	126.23	126.23	142.2	142.2
		109.3	109.3	117.13	117.13	102.7	102.7	118.89	118.89				
	4	382.82	204	382.82	201.56	369.9	149.76	369.9	137.68	395.78	168.02	395.78	187.24
		335.12	203.38	335.12	198.82	326.89	167.84	326.89	157.35	358.53	197.97	358.53	204.37
		313.94	207.28	313.94	195.8	304.69	183.3	304.69	176.19	324.23	197.1	324.23	208.34
		288.06	206.55	288.06	196.26	286.32	183.05	286.32	185	303.08	206.24	303.08	216.09
		243.03	189.67	243.03	182.82	250.56	186.72	250.56	190.28	291.6	214.44	291.6	228.62
		209.41	179.08	209.41	173.47	223.24	177.62	223.24	189.64	255.44	211.59	255.44	216.78
		187.13	170.73	187.13	167.85	181.98	160.16	181.98	166.57	229.61	202.55	229.61	210.19
		142.69	142.69	133.82	133.82	153.38	146.01	153.38	148.9	190.17	181.91	190.17	185.06
						125.97	125.97	146.48	146.48	168.86	168.86	178.66	178.66
1.0	1	350.79	123.83	350.79	95.27	333.56	75.69	333.56	93.44	356.47	117.56	356.47	111.1
		284.12	115.39	284.12	99.26	248.19	87.38	248.19	107.31	331.8	125	331.8	136.2
		275.79	111.27	275.79	97.07	180.72	81.04	180.72	99.24	306.92	122.45	306.92	139.41
		224.38	104.94	224.38	119.2	176.13	87.23	176.13	101.62	290.79	129.56	290.79	145.47
		200.77	111.66	200.77	126.62	141.07	89.35	141.07	101.79	253.72	125.89	253.72	144.34
		143.69	93.24	143.69	100.33	113.66	90.52	113.66	95.85	221.75	126.33	221.75	147.28
		98.63	98.63	116.78	116.78	86.13	77.75	86.13	79.46	170.92	117.18	170.92	136.03
						69.02	67.02	71.25	71.25	137.6	107.53	137.6	121.27
						53.88	53.88			101.47	101.47	118.19	118.19
	2	353.96	158.1	353.96	147.91	377.5	139.31	377.5	112.86	370.2	201.73	370.2	218.46
		325.7	163.33	325.7	166.15	329.61	149.16	329.61	122.48	328.45	199.2	328.45	211.96
		279.15	162.86	279.15	170.37	315.89	167.95	315.89	140.09	312.82	195.46	312.82	212.54
		255.76	163.37	255.76	169.28	275.46	172.75	275.46	151.52	277.22	198	277.22	212.11
		237.21	158.37	237.21	172.02	243	166.96	243	152.35	234.52	188.44	234.52	198.08
		206.17	152.05	206.17	165.52	208.13	158.65	208.13	148.18	201.82	181.94	201.82	187.63
		157.66	131.81	157.66	141.49	153.43	133.83	153.43	130.82	181.08	181.08	186.55	186.55
		135.88	123.96	135.88	128.74	119.38	114.56	119.38	113.65				
		113.56	113.56	124.25	124.25	103.7	103.7	106.85	106.85				
1.0	3	385.24	184.49	385.24	186.9	394.3	179.98	394.3	166.59	381.35	230.29	381.35	247.85
		335.13	195.72	335.13	209.42	349.51	189.96	349.51	182.38	336.67	240.62	336.67	251.03
		303.82	196.91	303.82	209.17	304.18	189.75	304.18	185.18	305.13	246.27	305.13	256.34
		271.29	190.11	271.29	207.08	291.12	191.69	291.12	192.56	253.14	231.92	253.14	234.01
		244.55	201.95	244.55	209.96	256.19	186.9	256.19	193.35	220.53	220.53	228.01	228.01
		221.37	194.22	221.37	204.07	196.7	161.92	196.7	171.08				
		182.89	182.89	201.44	201.44	174.06	153.17	174.06	162.64				
						144.47	144.47	161.35	161.35				
1.5	1	331.41	133.27	331.41	150.61	329.28	82.1	329.28	77.4	319.79	156.27	319.79	174.4
		303.5	140.02	303.5	156.67	311.49	108.6	311.49	104.36	296.82	185.43	296.82	192.35
		288.42	142.3	288.42	160.91	296.32	111.1	296.32	122.89	253.42	185.3	253.42	187.16
		243.57	138.09	243.57	154.27	263.55	113.07	263.55	120.03	183.52	157.59	183.52	161.52

Continued on next page

Table 1 – continued from previous page

Target Thickness (mm)	No. of layers	Blunt nosed Projectile				Ogive nosed projectile				Hemispherical nosed projectile			
		Observed		Predicted		Observed		Predicted		Observed		Predicted	
		IE	AE	IE	AE	IE	AE	IE	AE	IE	AE	IE	AE
		(Joule)				(Joule)				(Joule)			
		191.36	122.97	191.36	136.44	243.57	115.03	243.57	124.99	149.81	140.5	149.81	143.03
		133.94	107.46	133.94	113.09	206.74	117.91	206.74	126.65	126.76	126.76	135.33	135.33
		107.91	107.91	107.98	99.51	146.26	105.26	146.26	109.91				
				90.14	90.14	103.79	89.33	103.79	92.59				
						77.38	77.38	90.14	90.14				
	2	387.36	216.41	387.36	214.09	361.32	190.12	361.32	182.31	371.45	243.79	371.45	271.65
		344.16	223.17	344.16	216.05	318.43	199.22	318.43	187.16	350.95	260.36	350.95	279.45
		317.31	229.81	317.31	222.75	298.6	201.74	298.6	192.62	295.57	247.72	295.57	261.11
		252.48	210.1	252.48	200.04	251	191.56	251	195.55	245.71	245.71	257.9	257.9
		228.15	201.39	228.15	194.19	208.93	177.07	208.93	181.06				
		196.53	196.53	186.63	186.63	186.29	166.42	186.29	172.66				
						162.37	162.37	170.02	170.02				
2.0	1	389.25	168.86	389.25	186.42	420.18	200.96	420.18	193.06	377.03	200.37	377.03	193.82
		355.21	165.97	355.21	182.57	357.58	200.22	357.58	208.53	338.52	203.54	338.52	195.95
		308.25	159.75	308.25	180.61	325.32	199.02	325.32	209.54	316.15	201.69	316.15	204.01
		249.04	146.95	249.04	166.5	290.86	202.44	290.86	220.08	277.84	199.54	277.84	201.52
		202.69	139.37	202.69	153.42	240.66	184.59	240.66	196.28	243.69	195.79	243.69	201.06
		180.63	142.15	180.63	153.28	183.89	160.3	183.89	168.27	173.91	173.91	192.79	192.79
		116.76	116.76	134.57	134.57	118.37	118.37	148.44	148.44				
2.5	1	385.11	181.83	385.11	197.22	397.34	193.54	397.34	205.97	365.38	213.02	365.38	234.64
		355.41	182.72	355.41	206.34	364.55	200.59	364.55	219.11	299.62	222.17	299.62	237.03
		329.32	193.1	329.32	209.35	325.81	198.64	325.81	213.47	241.39	241.39	255.72	255.72
		293	193.27	293	208.8	279.06	193.7	279.06	210.5				
		259.16	193.12	259.16	207.85	245.71	202.5	245.71	210.87				
		199.83	171.87	199.83	180.69	165.29	165.29	200.52	200.52				
		145.42	145.42	165.49	165.49								
3.0	1	366.76	224.61	366.76	240.48	366.07	227.5	366.07	242.1	356.58	318.44	356.58	356.58
		351.94	232.61	351.94	241.8	331.77	236.01	331.77	240.95	307.19	307.19		
		344.58	234.1	344.58	244.9	292.82	257.43	292.82	261.74				
		307.29	219.63	307.29	233.36	263.64	243.59	263.64	248.08				
		269.35	217.97	269.35	227.57	246.48	235.15	246.48	238.07				
		230.21	205.12	230.21	213.57	214.69	214.69	234.92	234.92				
		200.03	200.03	218.33	218.33								

Finite element analysis of the present problem was carried using ABAQUS/ Explicit, an algorithm that is most suitable for problems involving very high rate of deformation in very short duration. The material behavior of the target in the numerical simulation was incorporated using Johnson and Cook [6, 7] elasto-viscoplastic model that is capable to predict the flow and fracture behavior of the target. The Von-Mises stress $\bar{\sigma}$ of the Johnson-Cook model includes the effect of three material characteristics namely strain hardening, strain rate hardening and temperature softening. Each of these three characteristics is incorporated independently in the equivalent stress equation that can be expressed as;

$$\bar{\sigma} = \left[A + B\left(\bar{\varepsilon}^{pl}\right)^{n}\right]\left[1 + Cln\left(\frac{\dot{\bar{\varepsilon}}^{pl}}{\dot{\bar{\varepsilon}}_0}\right)\right]\left(1 - \hat{T}^{m}\right) \tag{1}$$

where A, B, C, n, and m are material parameters, $\bar{\varepsilon}^{pl}$ is the equivalent plastic strain, $\dot{\bar{\varepsilon}}^{pl}$ is equivalent plastic strain rate, $\dot{\varepsilon}_0$ is a reference strain rate, and $\hat{T}$ is the non dimensional temperature expressed below;

$$\hat{T} = (T - T_0) / (T_{melt} - T_0) \;\; T_0 \leq T \leq T_{melt} \tag{2}$$

where T is the current temperature, T_{melt} is the melting point temperature, and T_0 is the room temperature.

The equivalent fracture strain equation of the Johnson-Cook model also incorporates the effect of three important material characteristics affecting the fracture of ductile material i.e. stress triaxiality, strain rate, and temperature as shown below;

$$\bar{\varepsilon}_f^{pl} = \left[D_1 + D_2 \exp\left(D_3 \frac{\sigma_m}{\bar{\sigma}}\right)\right] \left[1 + D_4 \, in \left(\frac{\dot{\bar{\varepsilon}}^{pl}}{\dot{\varepsilon}_0}\right)\right] \left(1 + D_5 \hat{T}\right) \tag{3}$$

where D_1 to D_5 are material constants and σ_m is the mean stress. Uni-axial tensile tests were carried out with round specimens to obtain modulus of elasticity(E), Poisson's ratio (v), yield stress (A), strain hardening parameter (B) and exponent (n). Notched specimens with three different notch radii, namely 2 mm, 0.8 mm and 0.4 mm were tested to obtain parameters D_1, D_2, D_3. Parameters C, m and D_4 were taken from Clausen et al. [1]. Parameter D_5, which incorporates the effect of temperature in the fracture strain was considered zero in the present investigation. The detail of each of the above parameter and its identification procedure is described in [11]. The numerical values of these parameters are given in Table 2.

The projectile was modeled as an analytical rigid body and the target plate as a deformable body. To reduce the computational cost of the analysis the projectile and the target plate was modeled as an axi-symmetric body. Surface to surface contact was assigned between the bullet and the target using kinematic contact algorithm. Effect of friction between the target and that of the projectile was considered negligible, however, a coefficient of friction of 0.5 was incorporated between contact surfaces of layered in contact target plates. The value of coefficient of friction was obtained from inclined plane experiments carried out in the laboratory. A small sheet of the used material was kept at a certain inclination and another piece of the same material was kept over it. The angle of inclination of the earlier was measured as soon as the later starts sliding. The value 0.5 is an average of the several experiments. A large number of elements was considered over the thickness of the target plate keeping aspect ratio of the elements close to one in the influenced region where the projectile comes in contact with that of the target. Four noded axi-symmetric quadrilateral elements were considered in the case of monolithic target plate impacted by flat, ogive and hemispherical nosed projectiles. In the case of layered target plate four noded quadrilateral elements were considered for the case of impact by blunt and hemispherical nosed projectiles. However, for ogive nosed projectile impact on layered target plate three noded axi-symmetric triangular elements were employed to avoid the distortion of elements that was more prominent in this case. Table 3 shows the number of elements used through the thickness of each target plate. The number of elements in the thickness of a layered plate and equivalent monolithic plate was considered identical. Adaptive meshing was also incorporated to avoid the distortion of the elements and for the smooth running of the program

Table 2: Material parameters used for Numerical Simulation of the Problem

Modulus of Elasticity, E (N/mm^2)	65.76 x10^3
Poisons ratio, v	0.3
Density, ρ (kg/m^3)	2700
Yield stress, A (N/mm^2)	148.36
B (N/mm^2)	345.51
η	0.18
C	0.001
Reference strain rate, $\dot{\varepsilon}_0$ (1/s)	1.0
m	0.85
T_{melt} (K)	893
T_0 (K)	293
Specific heat, C_p (J/kgK)	920
Inelastic heat fraction, η	0.9
D_1	0.07
D_2	1.24
D_3	-1.14
D_4	0.14
D_5	0.0

in all the cases of layered plates, and in the case of ogive and hemispherical nosed projectiles impact on single plates. Figure 2 shows the progress of deformation as well as Von-Mises stress contours of monolithic as well as layered target plates impacted by each of the three projectiles as a result of computational analysis. The predicted pattern of deformation is found to be identical in the case of blunt and hemispherical nosed projectiles. However, in the case of ogive nosed projectile impact the number of petals formed in the target plate could not be predicted by the code due to the axi-symmetric modeling of the structure.

3 Behavior of Target Plates Subject to Varying Impact Energy

A typical variation of the observed and predicted residual projectile energy as well as energy absorbed by the target plate as a result of increasing projectile impact energy is shown in Figs.3 and 4 for the monolithic and layered in-contact target plates respectively. During the experimental investigation the ballistic limit (the impact velocity at which the projectile was left with no residual velocity) of the projectile was initially obtained for each target plate. Afterward, the impact velocity of the projectile was increased in each consecutive shot. It was observed that with an increase in the impact energy the residual energy of the projectile

Table 3: Number of Elements through thickness of each target plate

Plate thickness (mm)	**Number of elements through thickness**
0.5	9
0.71	13
1.0	18
1.5	27
2.0	36
2.5	45
3.0	54

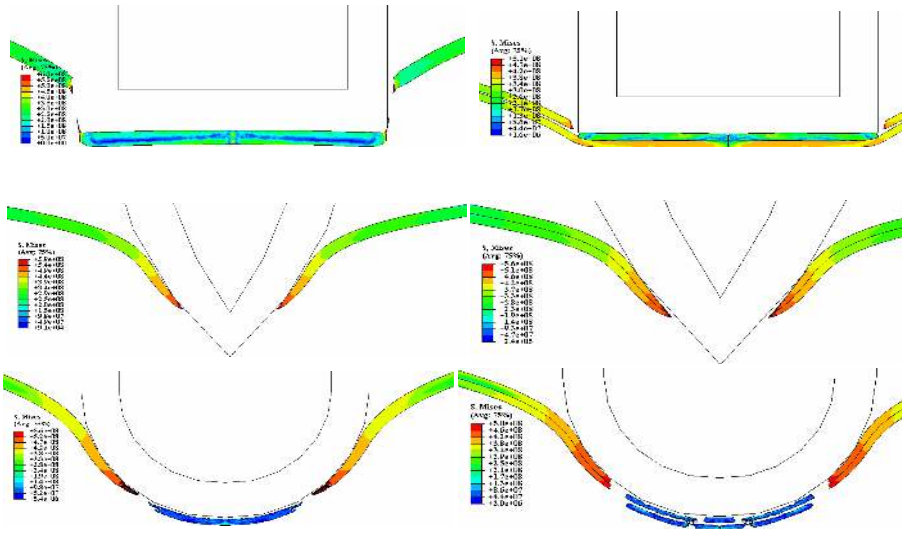

Figure 2: Variation of Von-Mises stress with the deformation of monolithic and layered target plates

increased almost linearly revealing an incessant decrease in the resistance of the target plate. This phenomenon was observed for all the cases of single and layered in-contact target plates impacted by each of the three projectiles. Nevertheless, the energy absorbed by the target plate (the difference between the impact energy and residual energy of the projectile) increased initially with an increase in the impact energy and reached to a maximum value. With further increase in the impact energy however, the energy absorbed by the target plate decreased slightly before it becomes almost constant. However, in a few cases of impact such as in the case of monolithic plate of 0.5 mm thickness as well as five layered plate of 0.5 mm thickness impacted by blunt nosed projectile, and, four layered plate of 0.71 mm thickness impacted by ogive and hemispherical nosed projectiles respectively, the absorbed energy increased initially up-to a maximum value and later it decreased monotonically. In the case of monolithic plate of 2.5 mm thickness impacted by hemispherical nosed projectile however, the energy absorbed by the target plate was found to decrease continuously with increasing impact energy. A similar investigation was carried out by [17], in which aluminum and mild steel plates were impacted by steel spheres in a velocity range of 150 to 2700 m/s. It was noticed that the velocity drop experienced by the projectile decreases from the ballistic limit to a minimum value and then it increases monotonically with increasing initial projectile velocity for all projectile and target systems. Furthermore, [16] studied penetration response of 12 mm Weldox steel plates impacted by flat, hemispherical and conical nosed projectiles. The change in projectile kinetic energy was evaluated and transformed into the total work done "W". It was observed that for blunt projectiles "W" increased continuously from the ballistic limit with increasing initial projectile velocity. However, for conical and hemispherical projectiles "W" decreased initially from a maximum value at the ballistic limit to a minimum value, and afterwards it further increased monotonically with increasing initial projectile velocity. The drop in "W" was found to be more distinct for conical projectile than that for the hemispherical projectile. The predicted results shown in the above mentioned figures (Figs. 3 & 4) also depict the same behavior as that of the experimental results. However, it has been found that when the target plate was hit at low impact energy, the predicted energy absorbed by the single as well as layered target plate is found to be more than that of the actual absorbed energy. However, as the impact energy was increased the predicted energy absorbed by the target plate was found to decrease and became more comparable to that of the actual absorbed energy. Moreover, with further increase of impact energy the predicted energy got stabilized. In a few cases however, such as in the case of single plate of 0.5 mm thickness impacted by blunt nosed projectile, and, five layered plate of 0.5 mm and four layered plate of 0.71 mm thickness impacted by ogive nosed projectile the predicted absorbed energy further decreased and became lower than that of the actual absorbed energy.

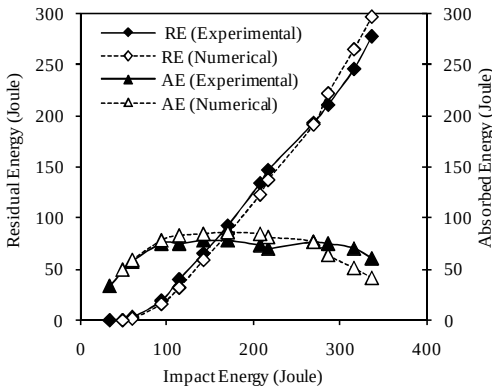

(a) 0.5 mm thick plate impacted by blunt nosed projectile

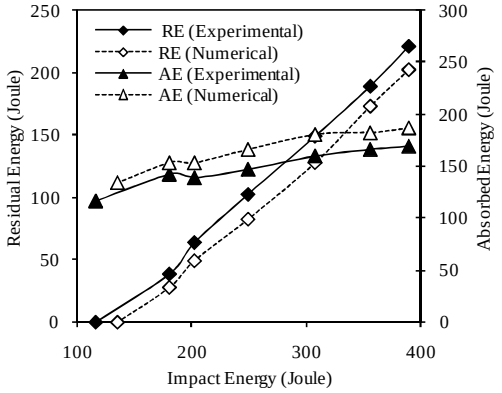

(b) 2 mm thick plate impacted by blunt nosed projectile

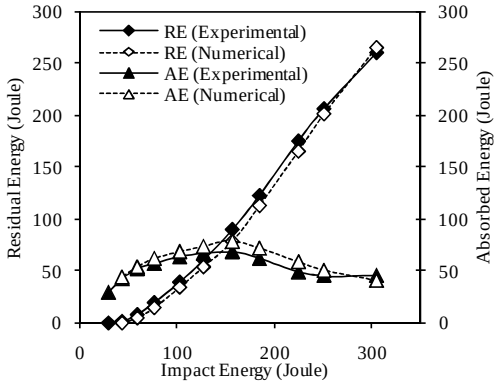

(c) 0.5 mm thick plate impacted by ogive nosed projectile

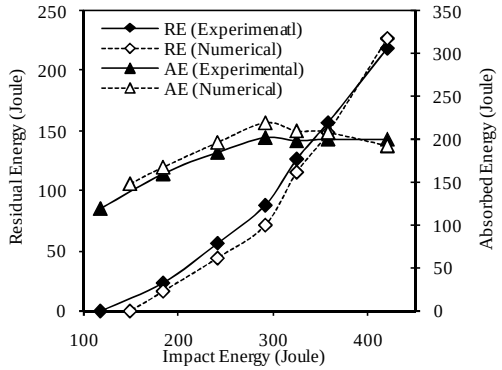

(d) 2 mm thick plate impacted by ogive nosed projectile

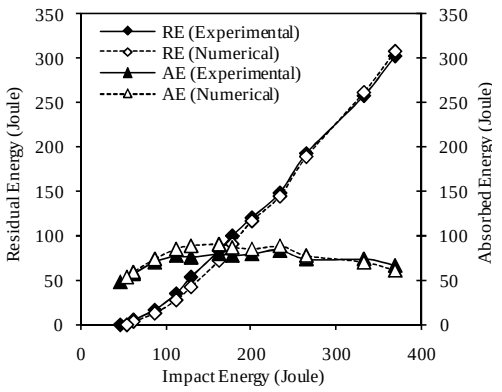

(e) 0.5 mm thick plate impacted by hemispherical nosed projectile

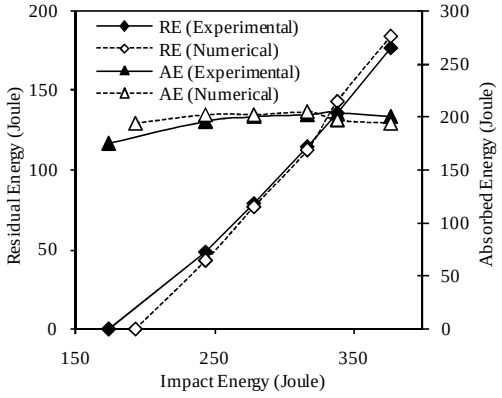

(f) 2 mm thick plate impacted by hemispherical nosed projectile

Figure 3: Variation of observed and predicted residual projectile energy (RE) as well as energy absorbed (AE) by the monolithic target plates

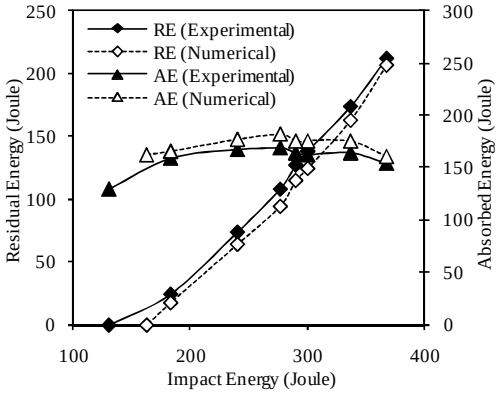

(a) Five layered plate of 0.5 mm thickness impacted by blunt nosed projectile

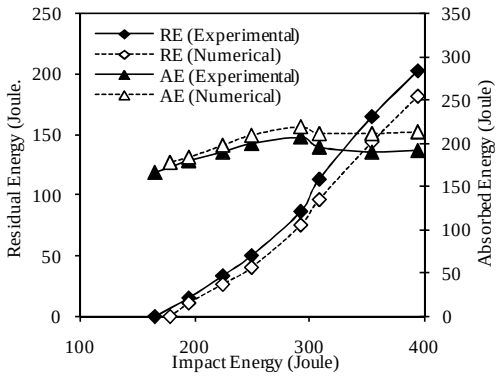

(b) Four layered plate of 0.71 mm thickness impacted by blunt nosed projectile

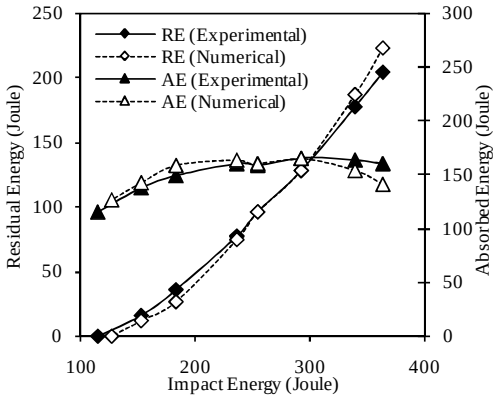

(c) Five layered plate 0.5 mm thickness impacted by ogive nosed projectile

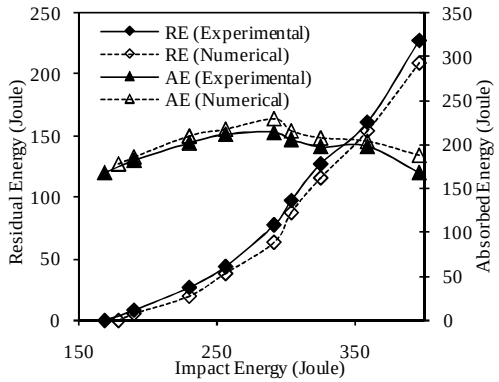

(d) Four layered plate 0.71 mm thickness impacted by ogive nosed projectile

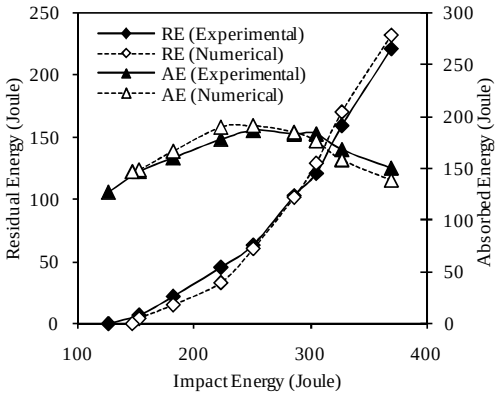

(e) Five layered plate 0.5 mm thickness impacted by hemispherical nosed projectile

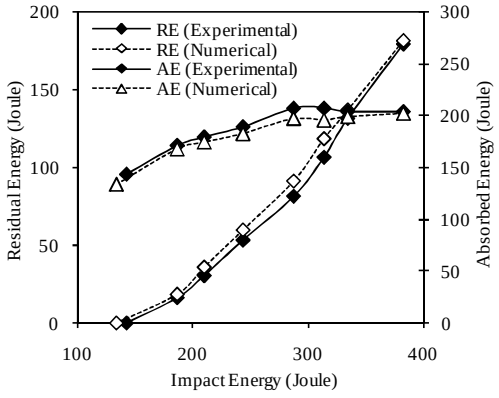

(f) Four layered plate 0.71 mm thickness impacted by hemispherical nosed projectile

Figure 4: Variation of observed and predicted residual projectile energy (RE) as well as energy absorbed (AE) by the layered in-contact target plates

4 Effect of Target Configuration

The configuration of a target may affect its failure mechanism which in turn may cause significant influence on its energy absorption capacity. It has been reported by several investigators [4, 9] that a single plate subjected to projectile impact is when replaced by several thin layered plates to give equivalent thickness the later has shown higher penetration resistance. However, studies in the literature have also revealed a contrast target behavior, according to which a monolithic target plate is found to be more efficient armor [10] than that of the layered in-contact plate of equivalent thickness. The above contradiction in the behavior of monolithic and layered targets may be due to a number of factors such as projectile and target geometry, total thickness of the monolithic and layered target, thickness of each layer in a layered target, target thickness to projectile diameter ratio and deformation behavior of the target. When a single plate subjected to impact by projectiles is replaced by several layered thin plates to give equivalent thickness, the mode of deformation may change from shearing to bending and membrane stretching of individual plates. This phenomenon may cause higher penetration resistance to the projectiles impacted on layered plates.

In the present study the significance of target configuration has been carefully investigated. The arrangement of the target plate was varied from single to layered plate with different number of layers giving equivalent overall target thickness. Different configurations of the target studied in the present investigation are shown in Table 4. Fig. 5 shows a typical comparison of observed and predicted energy absorption capacity of the target plates of total equivalent thickness 1.5, 2, 2.5 and 3 mm impacted by blunt, ogive and hemispherical nosed projectiles in different configurations. Three combinations of 1.5 mm total thickness (three layered plate of 0.5 mm thickness, two layered plate of 0.71 mm thickness and a monolithic plate of 1.5 mm thickness), four combinations of 2 mm total thickness (four layered plate of 0.5 mm thickness, three layered plate of 0.71 mm thickness, two layered plate of 1 mm thickness, and, a monolithic plate of 2 mm thickness), three combinations of 2.5 mm total thickness (five layered plate of 0.5 mm, four layered plate of 0.71 mm and monolithic plate of 2.5 mm thickness) and three combinations of 3 mm total thickness (three layered plate of 1 mm thickness, two layered plate of 1.5 mm thickness and monolithic plate of 3 mm thickness) were compared to ascertain the effect of number of layers on the energy absorption capacity of the target plate.

In general it was observed that as the number of layered plate decreases the resistance offered by the target plate increases; the monolithic target plate offered highest resistance against projectile perforation in the considered velocity regime. Failed layered targets showed bending but membrane stretching of each individual layer was not significant. The global deformation of the target plate was found to increase with an increase in the thickness of the target plate. Corran et al. [4] studied the behavior of mild steel, stainless steel and aluminum target plates impacted by projectile of different masses, nose shapes and hardness. It was observed that monolithic steel targets offered better resistance up to 3.5 mm thickness beyond which targets in two and three layers offered better resistance than equivalent monolithic target up to 6 mm

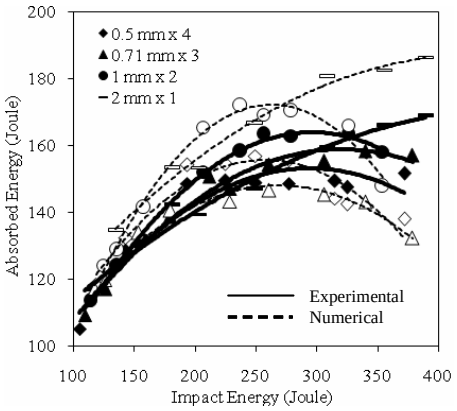

(a) Blunt nosed projectile case

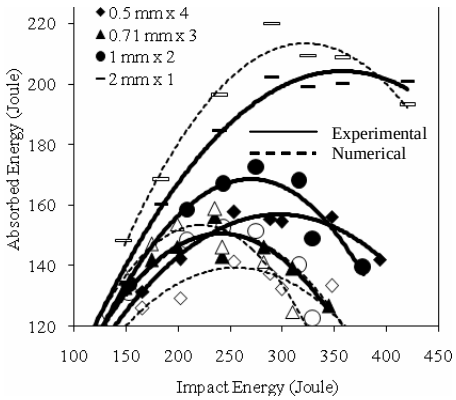

(b) Ogive nosed projectile case

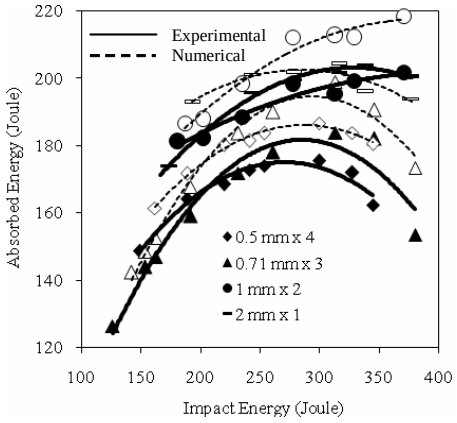

(c) Hemispherical nosed projectile case

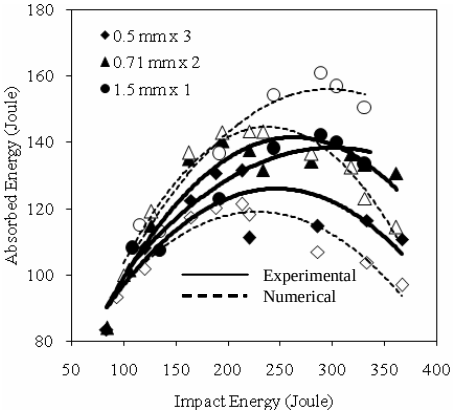

(d) Blunt nosed projectile case

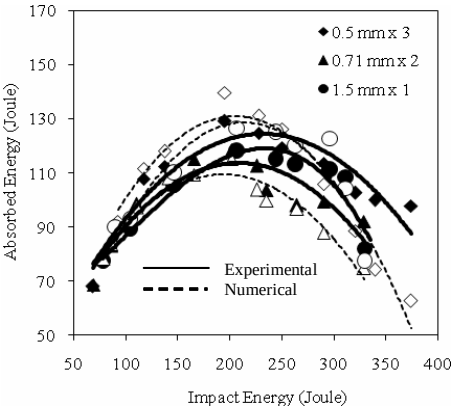

(e) Ogive nosed projectile case

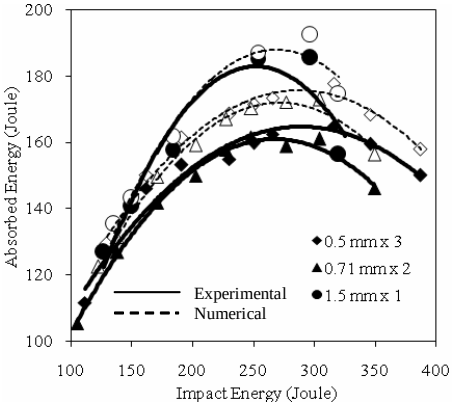

(f) Hemispherical nosed projectile case

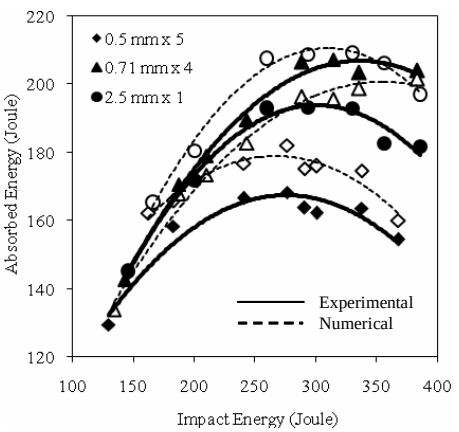

(g) Blunt nosed projectile case

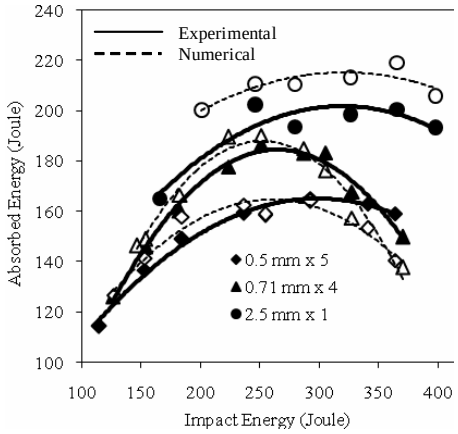

(h) Ogive nosed projectile case

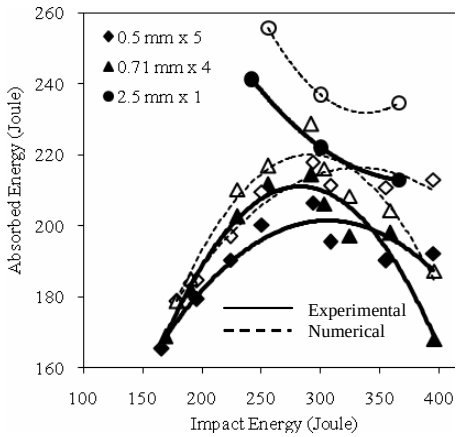

(i) Hemispherical nosed projectile case

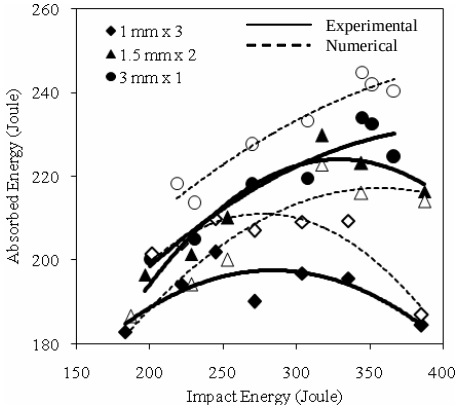

(j) Blunt nosed projectile case

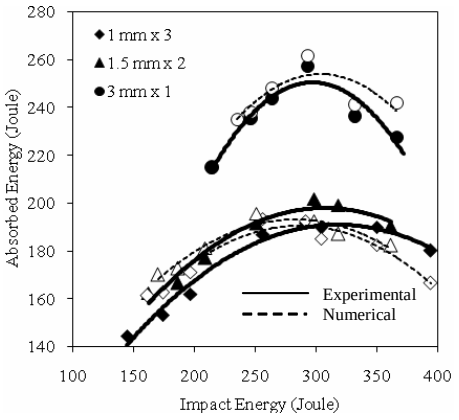

(k) Ogive nosed projectile case

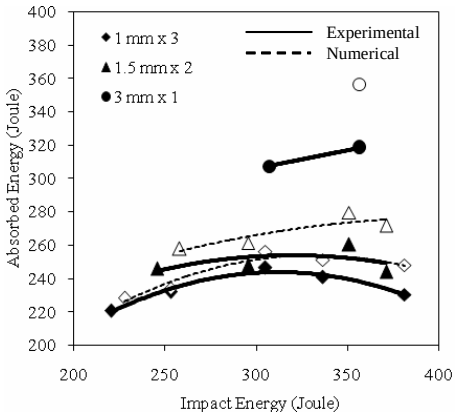

(l) Hemispherical nosed projectile case

Figure 5: Variation of observed and predicted energy absorption capacity of the target plates for varying target configuration

Table 4: Number of Elements through thickness of each target plate

Plate thickness (mm)	**Number of layers**
0.5	1
	2
	3
	4
	5
0.71	1
	2
	3
	4
1.0	1
	2
	3
1.5	1
	2
2.0	1
2.5	1
3.0	1

total thickness. It was also reported that the order of unequal thickness in layering the target is important. When thinner plate precedes the thicker one, the layered combination offers more resistance against perforation. Further, Zaid and Travis [3] (as reported by [10]) studied the capacity of single and layered steel plates of equivalent total thickness ranging from 1 to 9.5 mm when impacted by blunt projectiles. The very thin laminated plates exhibited less resistance than the equivalent single plate, but as the shield thickness increased the multiple plates became relatively more effective. Moreover, in the present investigation the global plastic deformation of layered targets was found to be lesser than that of the equivalent monolithic target except in the case of blunt nosed projectile impact. In a few cases of present investigation however, such as in the case of 2 mm equivalent thickness impacted by blunt and hemispherical nosed projectile [Figs. 5(a) and 5(b)] the two layered plate of 1 mm thickness is found comparable to that of the monolithic plate of 2 mm thickness. The same behavior is also observed in the case

of 1.5 mm equivalent target thickness impacted by blunt nosed projectile [Fig. 5(d)] in which case two layered plate of 0.71 mm thickness is found comparable to that of the monolithic plate of 1.5 mm thickness. In the case of 1.5 mm equivalent target thickness impacted by ogive nosed projectile [Fig. 5(e)] however, an opposite trend is observed which showed that three layered plate of 0.5 mm thickness absorbed highest kinetic energy followed by monolithic plate of 1.5 mm thickness and two layered plate of 0.71 mm thickness respectively. This contrary behavior of three layered plate of 0.5 mm thickness shows that its failure is governed by membrane stretching of individual plate. Figures 5(a)-(b) compare the energy absorption capacity of five layered plate of 0.5 mm thickness, four layered plate of 0.71 mm thickness and single plate of 2.5 mm thickness impacted by blunt, ogive and hemispherical nosed projectiles. For blunt nosed projectile impact, a four layered target with each layer of 0.71 mm thickness and 2.84 mm total thickness, offered highest perforation resistance. For ogive and hemispherical nosed projectile impact single plate of 2.5 mm thickness offered highest resistance. This particular case clearly revealed that there is considerable decrease in the resistance of the layered plate as compared to that of the monolithic plate. It is also observed from Fig. 5(i) that the energy absorbed by the monolithic plate of 2.5 mm thickness impacted by hemispherical nosed projectile decreases continuously with an increase in impact energy. In all the other cases however, the absorbed energy initially increased up to a certain level and later it decreased with increasing impact energy. In the case of monolithic plate of 3 mm thickness impacted by hemispherical nosed projectile [Fig. 5(l)] perforation was observed at 356.57 Joule impact energy (116.55 m/s velocity) below which the projectile failed to perforate the target plate. Numerical results however, showed that hemispherical nosed projectile could not perforate 3 mm thick plate at 116.55 m/s impact velocity.

5 Effect of Projectile Nose Shape

A review of impact studies carried out between 1978 and 1995, was presented by Corbet et al. [5]. It was concluded that the type of failure that occurs in the metals is primarily dependent on the projectile nose shape. It was also reported that thin ductile targets impacted by blunt nosed projectile fail through discing (thinning of the material under impact zone leading tensile tearing). Thick ductile targets however, fail through plugging (a shear dominated process in which a plug of the target material is separated). Sharp nosed projectiles cause failure of ductile targets of all thicknesses through ductile hole enlargement. In the present investigation the ductile failure was observed for 0.5 - 3 mm thick target plates. Blunt nosed projectile however, caused failure through shear plugging in all the cases of single and layered target plate, depicting somewhat different behavior from that observed by Corbet et al. [5]. Thinning of the target material was absent in this case and the plug that was removed from the plate was clean and circular without any deformation. Localised target deformation was also not found to be significant. The failure was severely affected by the blunt shape of the projectile nose, which

caused explicit shearing of the target material. The insignificant localised bending of the target material was a sign of resistance offered by the plate against shearing. After the detachment of the plug the target plate immediately failed without offering any resistance to the motion of the projectile.

Hemispherical nosed projectile failed the target plate through ductile hole enlargement. As the projectile came in contact of the target plate it pushed the material in front of its nose, which caused global as well as localised dishing, and, thinning of the contact region. After intensive thinning of the contact material a bowl shaped thin circular plug was ejected from the target plate. The material of the plug seemed to be strain-hardened, which may be a result of its severe thinning caused due to continuously being hammered by the projectile. To verify this observation the hardness of a 3 mm thick deformed plate and that of the plug ejected from it was measured. A small piece of the plate material was cut from the region towards the centre of plate. The Viker's hardness of the plug was measured to be 55.2 and that of the plate 41.1. Hemispherical nosed projectile also caused formation of small petals in the case of thinner monolithic as well as layered in contact plate. In the case of thicker plates however, petal formation was absent. Nose of the hemispherical projectile could only cause thinning of the material. It, being spherical in shape, could not play any significant role in tearing of the target material. Hence, all the kinetic energy of hemispherical nosed projectile was absorbed in the plastic flow of the target material which resulted in significant stretching and thinning and finally, rupture of the target material. Due to this reason hemispherical nosed projectile required highest energy to perforate both single as well as layered targets.

Ogive nosed projectile failed the target plates through ductile hole enlargement which is a common failure mode of ductile targets when impacted by pointed nosed projectiles. The projectile deformed the target plate in the form of its nose shape in the contact region, yet, it also caused uniform global bending of the target plate. The pointed tip of the projectile nose initially resulted in the formation of a minute hole in the target plate, which expanded due to the forward projectile pressure and development of high tensile stresses in the contact region, and caused formation of petals. The number of petals formed in the monolithic target plates was 4 in all the thicknesses. In most of the cases of layered target plates the number of petals was 5 in all the layers of a combination. However, in a few cases of layered plates the number of petals in the farthest layer was found to be 4, however, it remained 5 in all the other layers. The petals were bent by 90° from the surface of the plate. They were highly sharp and thinner at their tip. Thickness increases from the tip of petals to their base indicating extensive tensile stretching of target material. Bending of the target plate was also found to be significant, yet, it was lesser than in the case of target plate impacted by hemispherical nosed projectile. The nose shape of ogive nosed projectile played an important role to cause failure of target plate. Being pointed at its tip, it could easily pierce the target plate without significant dissipation of kinetic energy. Formation of petals as well as global bending of the target material was a process that occurred simultaneously after the tip of the projectile emerged out from the rear side of the plate. These two deformation mechanisms i.e. bending and petal formulation were affected

by radius of ogival shape that was 30° in the present case. It is reported in the literature that a decrease in the projectile nose radius increases the perforation efficiency of the ogive nosed projectile [5]. It may be due to the fact that as the nose radius of a projectile decreases, the area of the target in contact with that of the projectile will also decrease, due to which the projectile will require lesser energy to push the material in front of it in order to perforate the target.

The influence of projectile nose shape on the energy absorption capacity of the target plate has been illustrated by comparing the residual projectile energy as well as the energy absorbed by the single and layered target plates impacted by blunt, ogive and hemispherical nosed projectiles (Fig. 6(d)). The variation of absorbed energy with the thickness of target plate has also been compared for each of the three projectiles (Fig. 7). Both the monolithic and layered in-contact target plates showed considerably high resistance against perforation of hemispherical nosed projectile. The reason of which has been discussed earlier in this section. On the other hand the energy absorption capacity of the target plates against the impact of ogive and blunt nosed projectiles was found to be lesser as compared to that of the hemispherical nosed projectile. Thicker plates of 2, 2.5 and 3 mm thicknesses offered higher perforation resistance against ogive nosed projectile while thinner plates of 0.5, 0.71, 1.0 and 1.5 mm thicknesses offered better resistance against blunt nosed projectile impact. In the case of layered in-contact target plates however, ogive nosed projectile required least energy for perforation followed by blunt and hemispherical nosed projectiles respectively in all the cases investigated. Ogive nosed projectile failed targets through ductile hole enlargement by pushing the material aside through its nose. It required lesser energy to perforate thin targets ranging from 0.5 to 1.5 mm thickness and layered targets in which case also the thickness of each individual layer was varied from 0.5 to 1.5 mm. It may therefore be concluded that in a thin plate whether considered independently or in layered combination since lesser material was required to be pushed away by the ogival nose of the projectile therefore it required lesser energy for perforation. On the other hand in a thick monolithic plate the projectile is required to push more material in order to make its passage for perforation and therefore comparatively higher energy is consumed in this process. In a typical case of 3 mm thick monolithic target plate the ballistic limit velocity of blunt, ogive, and hemispherical nosed projectile was observed to be 87.294 m/s, 90.436 m/s and 108.178 m/s giving 200.03 Joule, 214.69 Joule and 307.19 Joule absorbed energy respectively by the target plates. In the case of two layered plate of 1.5 mm thickness however, the ballistic limit velocity was found to be 86.527m/s, 78.649 m/s and 96.75 m/s giving 196.53 Joule, 162.37 Joule and 245.71 joule energy absorbed by the target plates against the impact of blunt, ogive and hemispherical nosed projectiles respectively. The data clearly describes the effect of nose shape on energy absorption capacity of target plates. Moreover, it also signify the difference in the behavior of the monolithic and layered target plate (target configuration) discussed in the previous section. The influence of projectile nose on energy absorption capacity was also verified for varying target thickness, even though, no significant deviation was observed with the variation of target thickness, yet, it was confirmed that the ogive nosed projectile required lowest energy to perforate thinner target plate and blunt nosed projectile required lowest energy to perforate thicker target plate and

vise versa for monolithic plates [Fig. 7(a)]. It can be noticed from the figure that the curve of ogive nosed projectile is initially at the bottom, it however rises slowly after 1.5 mm thickness and becomes higher than that of the curve of blunt nose projectile. For layered in-contact plate however it was proved that, ogive nosed projectile required least energy to perforate all the combinations tested in the present investigation [Fig. 7(b)]. Hemispherical nosed projectile still remained least effective perforator. These facts were also studied through numerical simulation of the problem, the results of which are also presented in Figs 6-7 along with the actual results and depict same behavior of the target plate as is observed from the actual observations. Figure 8 shows the ballistic limit of different thicknesses of monolithic as well as layered target plates. It depicts a similar behavior of target plates through data points as is described in Fig. 7.

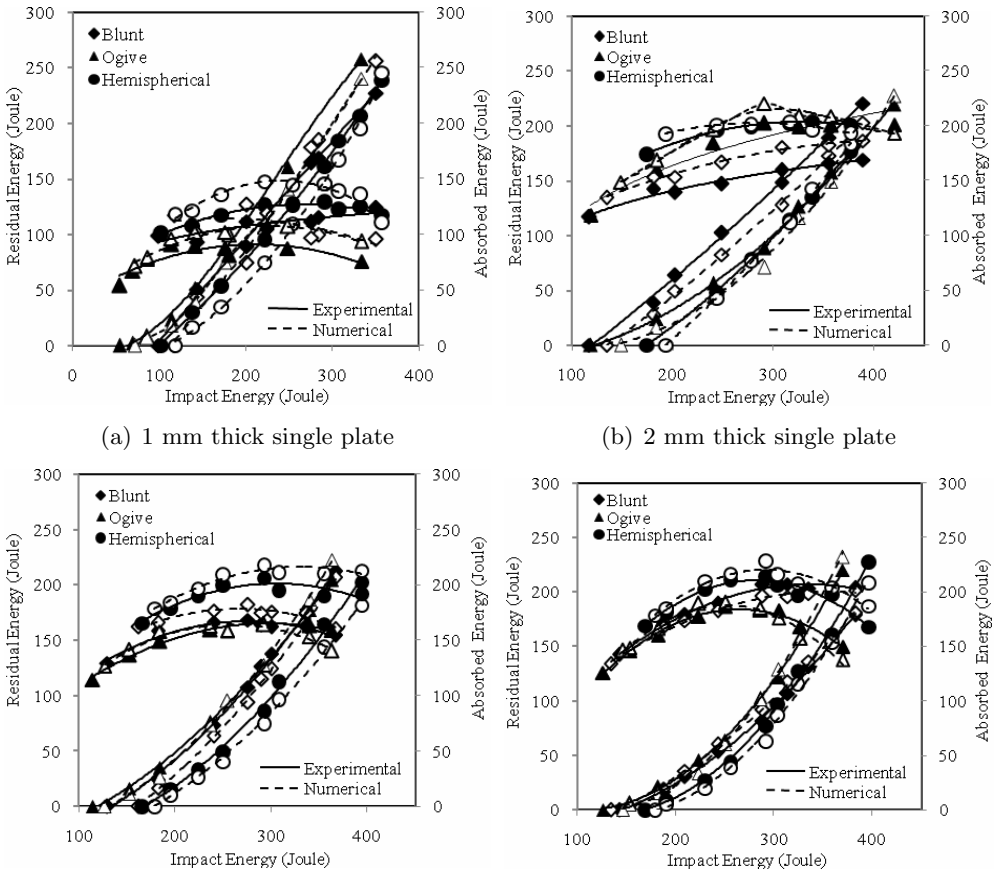

(a) 1 mm thick single plate

(b) 2 mm thick single plate

(c) Five layered plate of 0.5 mm thickness

(d) Four layered plate of 0.71 mm thickness

Figure 6: Comparison of observed and predicted residual projectile energy as well as energy absorbed by the target plates for different projectile noses

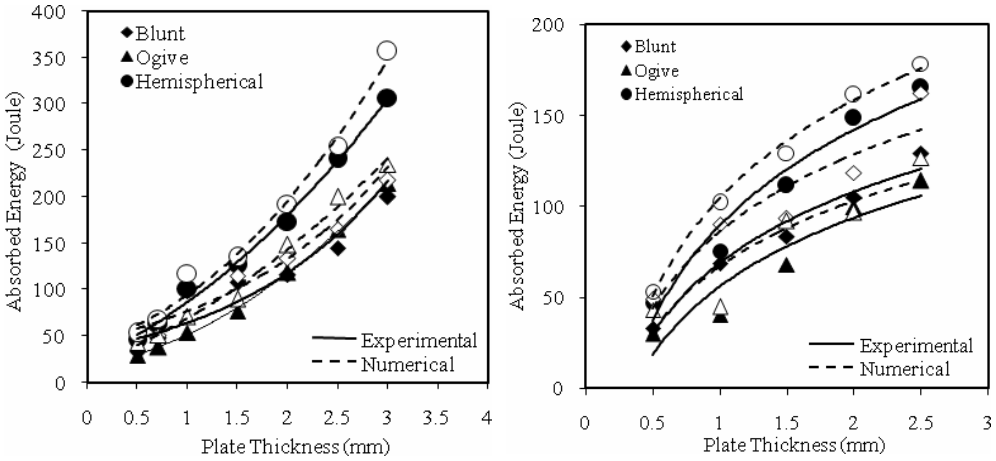

(a) Monolithic target plate (b) Five layered plate of 0.5 mm thickness

Figure 7: Variation of energy absorbed by the target plates with increasing target thickness for different projectile noses

6 Effect of Varying Thickness of Single and Layered Target Plates

Thickness of the target plate is another important parameter which has a considerable influence on its energy absorption behavior. Corran et al. [4] studied the energy absorption behavior of steel plates impacted by blunt projectiles. Four empirical equations were used to relate the energy absorption mechanism with the thickness of the target plate. It was concluded that the amount of plastic bending work increases with increase of plate thickness to maximum and thereafter it decreases sharply. The extent of elastic energy decreases with increase of plate thickness to minimum and then it increases. The amount of work absorbed in projectile deformation increases with increase of plate thickness. In the present investigation also an effort has been made to enlighten the role of plate thickness on the energy absorption capacity of the target plate. Fig. 9 illustrates the behavior of monolithic target with increasing thickness. Observed as well as predicted absorbed energies of the target plate are plotted for varying plate thickness (Fig. 9) for the case of blunt, ogive and hemispherical nosed projectiles respectively. The energy absorption behavior of layered target plate is also depicted in the same fashion in Fig. 10 for a few typical cases of varying number of layers of 0.5 mm and 0.71 mm thicknesses. The variation of ballistic limit velocity of each of the three projectiles with increasing target thickness is also shown in the figures to acquire clear understanding of target behavior. The absorbed energies shown in these figures are those obtained at the ballistic limit. Therefore, they may be referred as the minimum energy absorbed by the target plate, since, the energy absorption capacity of the target plate is found to increase with an increase in the projectile impact energy. However, after reaching a peak value the absorbed energy further decreased, yet,

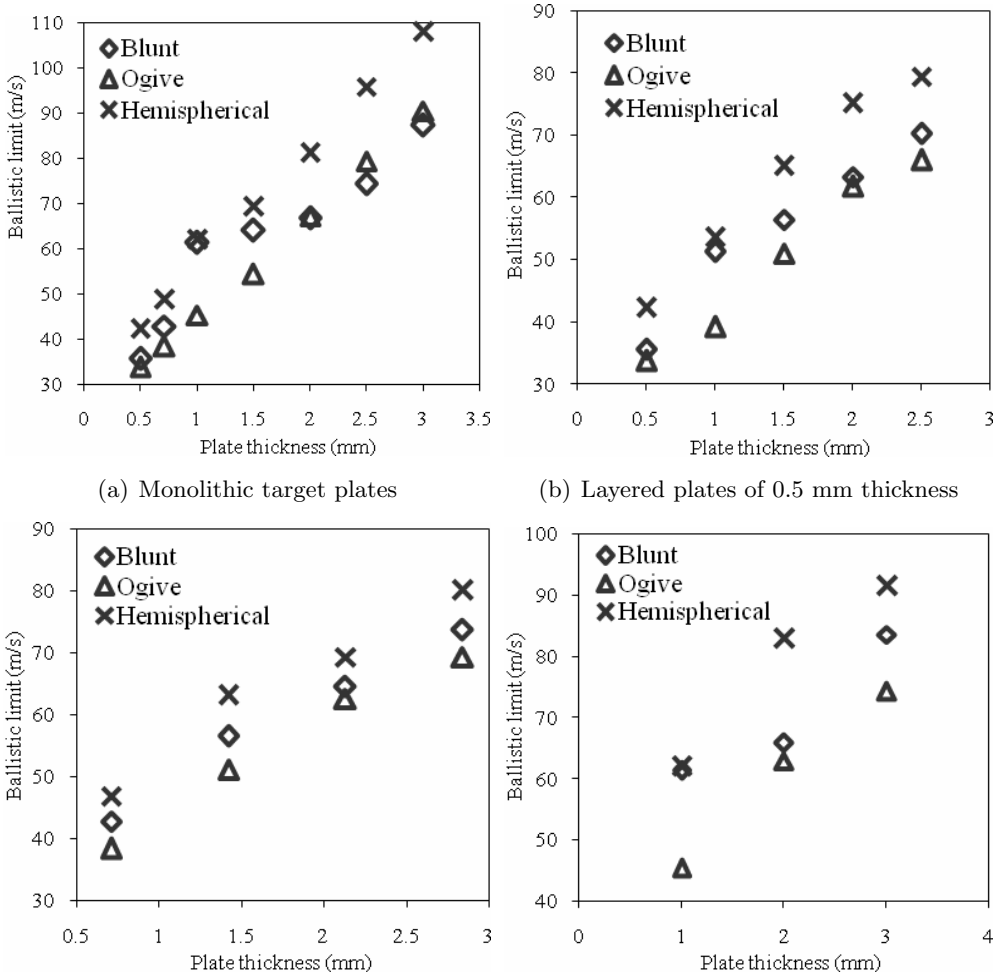

(a) Monolithic target plates

(b) Layered plates of 0.5 mm thickness

(c) Layered plates of 0.71 mm thickness

(d) Layered plates of 1.0 mm thickness

Figure 8: Observed ballistic limit of monolithic and layered target plates of different thicknesses

it still remained higher than that of the energy absorbed by the target plate at lowest impact energy (i.e. at the ballistic limit) except in the case of four layered plate of 0.71 mm thickness and two layered plate of 1.5 mm thickness impacted by hemispherical nosed projectile. Moreover, in the case of 2.5 mm thick monolithic plate impacted by hemispherical nosed projectile the absorbed energy decreased continuously with an increase in the impact energy. The experiments carried out by [13,16] with different nose shaped projectiles to study the strength of 12 mm thick steel plates revealed a similar behavior of the target plates. The energy absorption capacity of Weldox 460 E, Weldox 700 E and Weldox 900 E steel plates impacted by blunt nosed projectile increased with an increase of projectile impact energy. Weldox 460 E steel plates impacted by hemispherical nosed projectile, and Weldox700 E steel plates impacted by ogival and conical nosed projectiles also depicted a similar energy absorption behavior. On the other hand Weldox 460 E steel plates impacted by conical nosed projectiles showed a continuous decrease in the energy absorption capacity with increasing impact energy. In general it can be concluded from Figs. 9 and 10 that the energy absorption capacity increases more rapidly at higher thicknesses in the case of monolithic target plates. In the case of layered target plates the increase in the energy absorption capacity is more or less constant with each additional layer. The Predicted absorbed energy is found to be higher in all the cases of single as well as layered target plate. However, a good agreement can be seen between the observed and predicted results. Fig. 11 shows the variation of maximum plate deflection of the monolithic target plates with an increase in the projectile impact energy. The deformation of the target plates was measured with the help of mechanical dial gauge system. It is observed that the global plastic deformation of the target plates decreases with an increase in impact energy. Highest plastic deformation of the target plates was observed at ballistic limit velocity for all the three projectile nose shapes. The decrease of plate deflection with increasing impact energy is found to be more rapid in the case of target plates impacted by blunt nosed projectile. On the other hand, hemispherical nosed projectile showed more gradual decrease in the plate deflection with increasing impact energy. Nevertheless, the deflection of the target plates is found to be highest as a result of impact by hemispherical nosed projectile followed by ogive and blunt nosed projectiles respectively. Fig. 11 also revealed another important phenomenon that the global plastic deformation of the target plate increases with increase in its thickness. In the case of blunt nosed projectile impact however, the deflection of 0.5 mm thick target plate is found to be higher than that of the of 0.71 and 1.5 mm thicknesses. Moreover, in the case of hemispherical nosed projectile impact the deflection of 1.5 mm thick target plate is found to be comparable to that of the 0.5 and 0.71 mm thicknesses.

7 Conclusions

This paper presented a detailed experimental and finite element investigation of energy absorption behavior of single and layered aluminum target plates of thicknesses 0.5 to 3 mm impacted

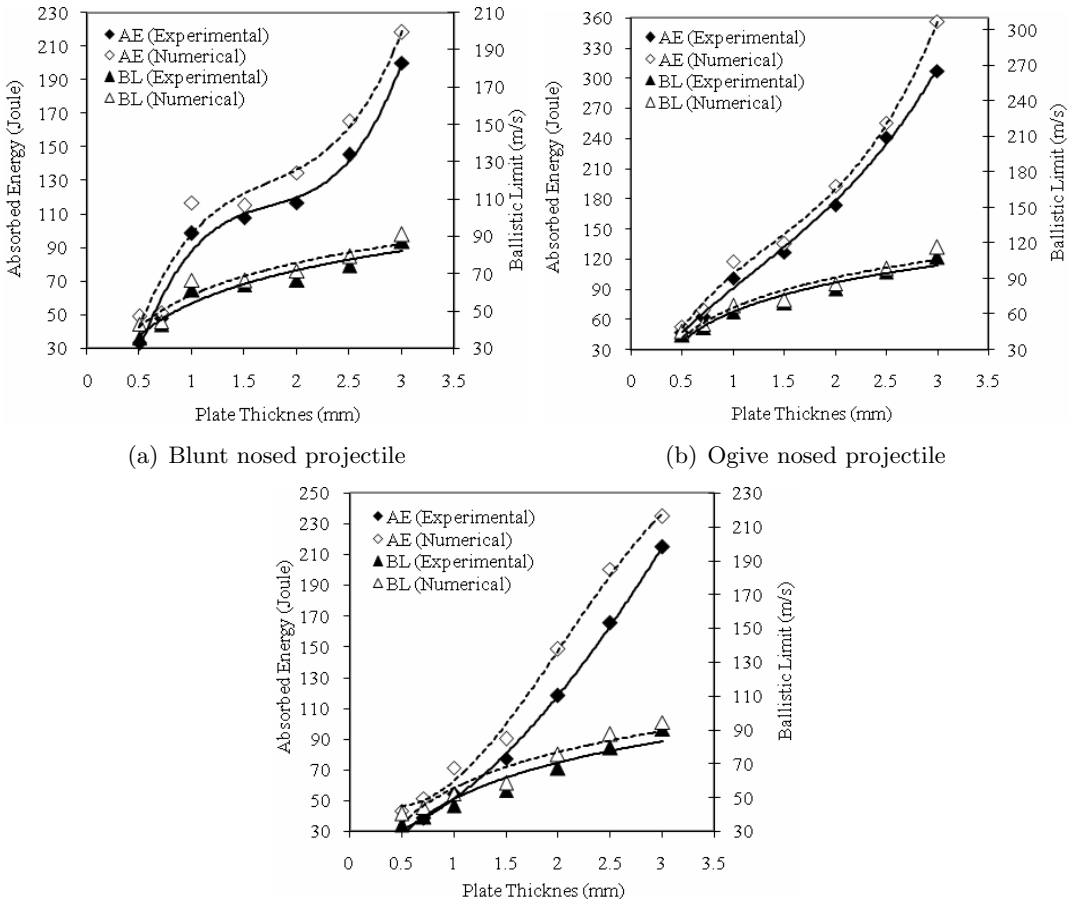

(a) Blunt nosed projectile

(b) Ogive nosed projectile

(c) Hemispherical nosed projectile case

Figure 9: Variation of absorbed energy as well as ballistic limit velocity with plate thickness of monolithic target plates

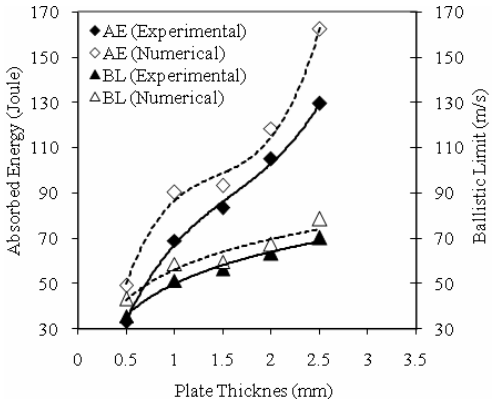

(a) Five layered plate of 0.5 mm thickness impacted by blunt nosed projectile

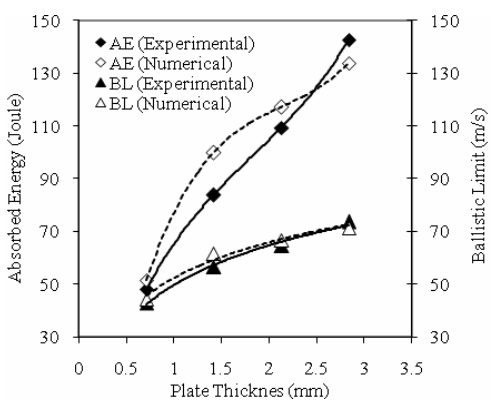

(b) Four layered plate of 0.71 mm thickness impacted by blunt nosed projectile

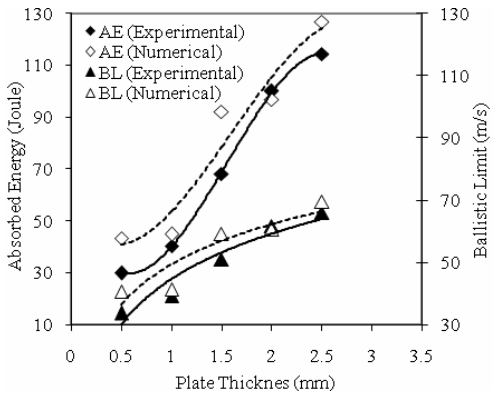

(c) Five layered plate of 0.5 mm thickness impacted by ogive nosed projectile

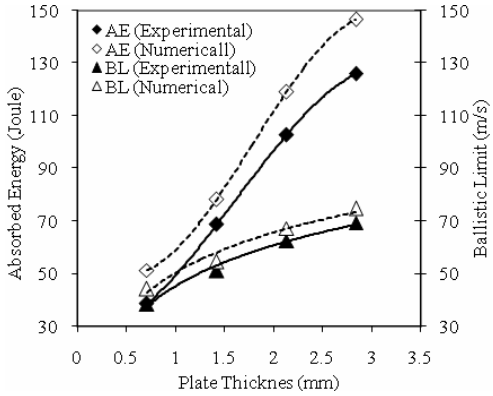

(d) Four layered plate of 0.71 mm thickness impacted by ogive nosed projectile

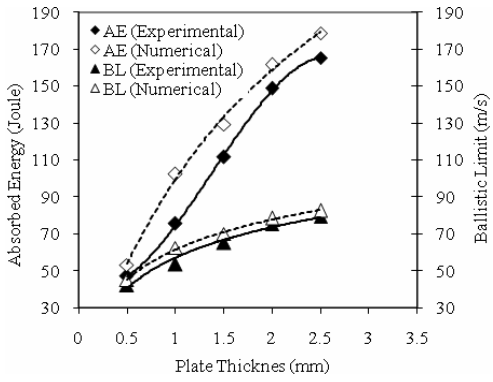

(e) Five layered plate of 0.5 mm thickness impacted by hemispherical nosed projectile

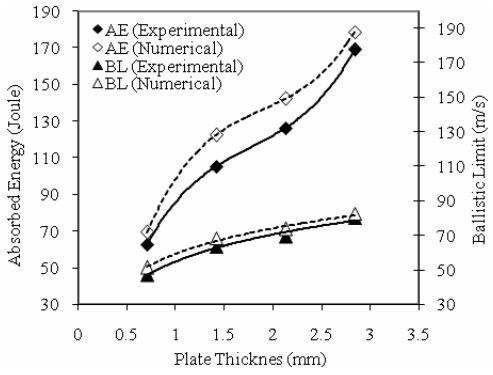

(f) Four layered plate of 0.71 mm thickness impacted by hemispherical nosed projectile

Figure 10: Variation of absorbed energy as well as ballistic limit velocity with plate thickness of layered in-contact target plates

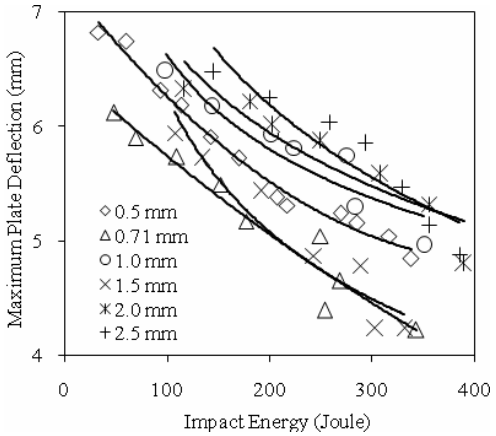

(a) Blunt nosed projectile case

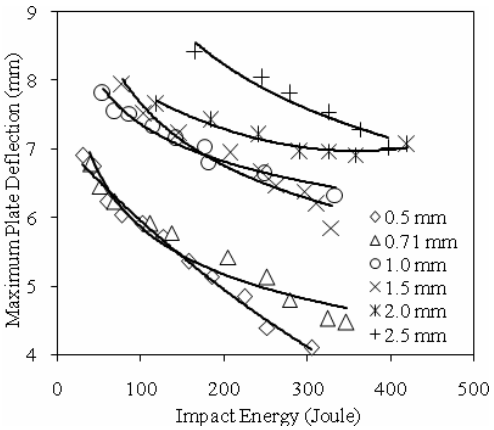

(b) Ogive nosed projectile case

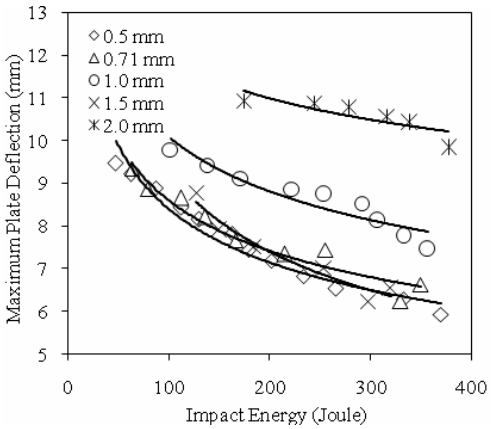

(c) Hemispherical nosed projectile case

Figure 11: Variation of maximum target deflection of the monolithic target plates with projectile impact energy

normally by blunt, ogive and hemispherical nosed projectiles in the velocity range of 33-136 m/s. Various parameters affecting the energy absorption behavior of the target plate such as kinetic energy of the impacting projectile, its nose shape, configuration of the target plate, failure mechanism as well as thickness of the target plate were investigated. Results obtained from the finite element analysis using the finite element code ABAQUS/Explicit were found to be in good agreement with those of the experimental results, however, they over predicted the energy absorption capacity of the single as well as layered target plates.

The residual energy of the impacting projectile increased linearly with increase in the impact energy. The energy absorbed by the target plate however, increased initially with the increase in impact energy and reached a peak value from where it decreased with further increase in the impact energy and finally got stabilized.

As the number of layers decreased the resistance offered by the target plate increased, the monolithic target offered highest resistance against projectile perforation.

Blunt nosed projectile failed the target plate through shearing while ogive and hemispherical nosed projectile through ductile hole enlargement, however, tensile stretching was much more prominent in the case of impact by hemispherical nosed projectile than in the case of the ogive nosed projectile. Hemispherical nosed projectile caused highest plastic deformation of the target plates followed by ogive and blunt nosed projectiles respectively. Due to the same reason the energy absorption capacity of the single and layered target plates was found to be highest as a result of impact by hemispherical nosed projectile. Thin monolithic plates of 0.5, 0.71, 1.0 and 1.5 mm thicknesses showed better resistance against the perforation by blunt nosed projectile while for thicker plates of 2.0, 2.5 and 3.0 mm thicknesses the same was found true for the case of ogive nosed projectile. Layered in-contact target plates however, offered lowest resistance against the impact of ogive nosed projectile in all the cases.

The maximum deflection of the target decreased with increase in the impact energy; this decrease was seen to be more rapid in the case of impact by blunt nosed projectile when compared with the results of impact by hemispherical nosed projectile. The global deformation of the target plate was found to increase with increase in its thickness.

References

[1] Clausen AH, Borvik T, Hopperstad OS, and Benallal A. Flow and fracture characteristics of aluminium alloy aa5083 h116 as function of strain rate, temperature and triaxiality. Mat Sci Engng, A364:260–272, 2004.

[2] Zaid AIO, EL-Kalay A, and Travis FW. An examination of the perforation of mild steel plates by a flat-ended cylindrical projectile. International Journal of Mechanical Sciences, 15:129–143, 1973.

[3] Zaid AIO and Travis FW. Conference on the mechanical properties of high rates of strain. Institution of Physics, pages 417–428, 1974. Conference serial no. 21.

[4] Corran, RSJ, Shadbolt PJ, and Ruiz C. Impact loading of platesan experimental investigation. International Journal of Impact Engineering, 1(1):3–22, 1983.

[5] Corbet GG, Reid SR, and Johnson W. Impact loading of plates and shells by free-flying projectiles: a review. International Journal of Impact Engineering, 18:141–230, 1996.

[6] Johnson GR and Cook WH. A constitutive model and data for metals subjected to large strains, high strain rates and high temperatures. In: Proceedings of the seventh International symposium on Ballistics, The Hague, 1983.

[7] Johnson GR and Cook WH. Fracture characteristics of three metals subjected to various strains, strain rates, temperatures and pressures. Engineering Fracture Mechanics, 21(1):31–48, 1985.

[8] Wen H-M and Jones N. Semi-empirical equations for the perforation of plates struck by a mass. in: Structures under shock and impact ii. Computational Mechanics Publications, page 369380, 1992.

[9] Marom I and Bonder SR. Projectile perforation of multi-layered beams. int. Journal of Mechanical Sciences, 21:489–504, 1979.

[10] Radin J and Goldsmith W. Normal projectile penetration and perforation of layered targets. International Journal of Impact Engineering, 7:229–259, 1988.

[11] Gupta NK, Iqbal MA, and Sekhon GS. Experimental and numerical studies on the behavior of thin aluminum plates subjected to impact by blunt- and hemispherical- nosed projectiles. International Journal of Impact Engineering, 32:1921–1944, 2006.

[12] Gupta NK, Iqbal MA, and Sekhon GS. Effect of projectile nose shape, impact velocity and target thickness on deformation behavior of aluminum plates. International Journal of Solids and Structures, 44:3411–3439, 2007.

[13] Dey S, Borvik T, Hopperstad OS, Leinum JR, and Langseth M. The effect of target strength on the perforation of steel plates using three different projectile nose shapes. International Journal of Impact Engineering, 30:1005–1038, 2004.

[14] Dey S, Borvik T, Teng X, Wierzbicki T, and Hopperstad OS. On the ballistic resistance of double-layered steel plates: An experimental and numerical investigation. JInternational Journal of Solids and Structures, 44:6701–6723, 2007.

[15] Othe S, Yoshizawa H, Chiba N, and Shida S. Impact strength of steel plates struck by projectiles. Bulletin JSME, 25(205):1226–12231, 1982.

[16] Borvik T, Langseth M, Hopperstad OS, and Malo KA. Perforation of 12mm thick steel plates by 20mm diameter projectiles with flat, hemispherical and conical noses part i: Experimental study. International Journal of Impact Engineering, 27:19–35, 2002.

[17] Goldsmith W and Finnegan SA. Penetration and perforation processes in metal targets at and above ballistic velocities. International Journal of Mechanical Sciences, 13:843–866, 1971.